Article

Topology Structural Design and Thermal Characteristics Analysis of High-Efficiency Heat Conductive Path for the Spindle System

Yang Li [1,*] **, Zhongting Liu** [2] **, Lei Li** [2] **, Wenlei He** [2] **, Zhaoyang Hou** [2] **, Wanhua Zhao** [1] **and Wenwu Wu** [3]

1   State Key Laboratory for Manufacturing Systems Engineering, Xi'an Jiaotong University, Xi'an 710054, China; whzhao@mail.xjtu.edu.cn
2   School of Mechanical Engineering, Xi'an Jiaotong University, Xi'an 710054, China; lzt15835760264@163.com (Z.L.); 3122301239@stu.xjtu.edu.cn (L.L.); 3121301119@stu.xjtu.edu.cn (W.H.); houzhaoyang@stu.xjtu.edu.cn (Z.H.)
3   Key Laboratory of NC Machine Tools and Integrated Manufacturing Equipment of the Education Ministry & Key Laboratory of Manufacturing Equipment of Shaanxi Province, Xi'an 710048, China; wuwen@xaut.edu.cn
*   Correspondence: liyangxx@xjtu.edu.cn; Tel.: +86-139-9113-2442

Abstract: In order to enhance the heat dissipation of the spindle under working condition, thermal conductivity paths were designed based on the topology optimization method. The heat conductive path was proposed to be constructed in the bearing housing and the spindle housing, which was simplified as a toroidal model. Taking the heat dissipation weakness as the optimization objective, the topological structure with the highest thermal conductivity was obtained based on the OC and IPTO algorithms. In order to analyze the influence of the heat conductive path on the circumferential heat distribution of the spindle, the thermal characteristic of the model with heat conductive paths filled with copper was investigated. Compared with the general model, the heat conductive path could reduce the temperature of the spindle from 47 °C to 33 °C when the volume proportion of the high thermal conductivity material was 40%. At the same time, the strength of the heat conductive path was analyzed, and the size of the stress was not more than 3MPa, which verified the effectiveness of the heat conductive path for efficient heat conduction.

Keywords: machine tool error; heat conductive path; continuum structure; topology optimization

1. Introduction

With the development of industrial technology, requirements for machining accuracy are becoming more and more demanding. In the process of high-speed and high-precision machining, thermal errors account for 40% to 70% of the total error of the machine tool [1–3]. During the high-speed operation of the machine tool, the electric spindle rotates at high speed, which generates a lot of heat due to the motor loss, friction between the rolling body, and the inner and outer rings of the bearing. The heat flows into different parts of the spindle system in different directions and rates, making the temperature field of the whole spindle system unevenly distributed. This leads to thermal errors along the axial and radial directions of the spindle [4–6]. Therefore, the spindle was considered one of the most important heat sources of the machine tool [7], and the thermal characteristics of the spindle directly influence the machining accuracy [8].

Traditionally, the spindle system is equipped with a cooling device in which there is a cooling water jacket [9]. It is installed outside the bearing to help reduce the temperature rise by convection [10,11]. In order to reduce the temperature rise, shorten the thermal equilibrium time, and even out the heat distribution, it was proposed to build a heat conductive path with one end contacting with the outer ring of the spindle bearing or the motor stator, and the other end connecting the external cooling system. The heat conductive path was filled with high heat conductivity material. It looks like a "highway" along which

the heat generated by the heat source inside the spindle could be exported to the bearing housing and the outside of the casing directly and quickly. In order enhance the heat transfer efficiency, the structure of the heat conductive paths should be designed properly.

Most scholars have studied the effect of geometric parameters on thermal resistance. By changing the shape and dimensional parameters of the heat conductive path [12,13], the thermal conductivity could be improved and the optimal solution could be obtained. There are numerous research methods such as bionic, conformal, and topological optimization. Cheng [14] used a bionic optimization method to optimize the arrangement of high thermal conductivity materials inserted in a certain region. The evolution and degradation process of high thermal conductivity materials have been simulated numerically. Peng [15] proposed a liquid-absorbing core structure based on the plant leaf vein system in 2015 and analyzed its fractal parameters and geometry. Then, the performance of the homogeneous thermal plate was successfully improved. The bionic methods play a certain role in heat dissipation, but the application scenarios of such bionic methods are limited, and the design ideas are mostly inspired by the phenomenon, which makes it difficult to do sustained research. Wang [16] established a three-dimensional heat dissipation model in 2019 and carried out the conformation design with thermal conductivity distribution and heat source intensity score as design variables, and the maximum system temperature and equivalent thermal resistance as performance indexes. Li [17] selected the minimization of maximum thermal resistance as the optimization objective and the aspect ratio of the end face of the heat sink unit as the optimization variables to optimize the structure of the composite heat sink in 2021. In configuration optimization, the relevant laws are often sought for the objective and design variables to adjust the structure accordingly. This method has the problem of a complicated solution and sometimes it is difficult to adjust the structure accordingly.

Topological optimization methods are the classical approach to structural optimization. In 1994, by combining topology optimization methods, Sigmund conducted homogenization design. Since then, the development of microstructure topology optimization design has been greatly promoted, and various metamaterial designs have emerged, such as microstructure design for specific performance materials and microstructure design for extreme performance materials [18–23]. In recent years, as people's demands for heat dissipation performance have gradually become higher, a large number of scholars have found that topological complementary methods are very effective in constructing highly efficient thermal conductive structures. Long and Jia [24,25] established a periodic structural topology optimization model based on the independent continuous mapping method to obtain an optimized microstructural configuration for the steady state thermal conductivity of composite materials. Zhao [26] used the topological complement optimization method and introduced the discrete body filtering method to obtain the circular path structure on the cross section of the mold. Based on the SIMP method, the thermal conductivity structure of IGBT for power devices was designed. Compared with the original IGBT module, it showed that the maximum junction temperature of the topological model decreased by 45.63% and the maximum equivalent thermal stress decreased by 40.35% [27].

The main contributions of this paper are:

(1)　For the first time, the heat path structure was constructed by means of topological optimization and applied to the heat dissipation of machine tool spindles, which can effectively increase the heat dissipation of the machine tool and reduce the thermal error of the machine tool by exporting the heat from the heat source and preventing the heat from spreading.

(2)　A topological solution method for the thermal path was proposed. Taking the heat dissipation weakness as the objective function, based on the SIMP interpolation model, combined with the IPTO and OC algorithms, the optimized discrete mathematical model was solved.

(3)　A three-dimensional model was established to analyze the thermal characteristics of the heat conductive path, and the thermal performance of the heat conductive

path obtained based on the two algorithms was compared under different volume proportions of high thermal conductivity materials.

In this paper, we attempted to use heat conductive paths in a machine tool spindle system for improving the efficiency of heat dissipation. Based on the topology optimization method, the best distributions of the paths were obtained. The thermal characteristics of the model with and without heat conductive paths were analyzed. The strength properties of the structure were also verified.

## 2. Mathematical Model of Heat Conductive Path

2.1. Centralized Thermal Conductivity Model

During the high-speed operation of the spindle, a lot of heat was generated due to the friction of the front and rear end bearings. The heat conductive path was proposed to be constructed in the bearing housing and the spindle housing to enhance heat transfer efficiency. Supposing NSK 7010C angular contact ball bearing is adopted in the spindle system, its contact angle is 15°, the size is $50 \times 80 \times 16$ mm, and the span of front and rear bearing is 300 mm. The total axial preload force is set as 300 N, the lubrication method is grease lubrication. The relevant parameters are shown in Table 1.

**Table 1.** Parameters of angular contact ball bearing (NSK 7010C).

Inner Diameter/d	Outer Diameter/D	Width/B	Highest Running Speed (Oil Lubrication)	Weight	C_{0r}	C_r
50 mm	80 mm	16 mm	17,700 r/min	0.259 kg	21.9 kN	26 kN

The area colored as red in the spindle system as shown in Figure 1 was selected as the design area for building heat conductive paths. It was simplified as the toroidal model.
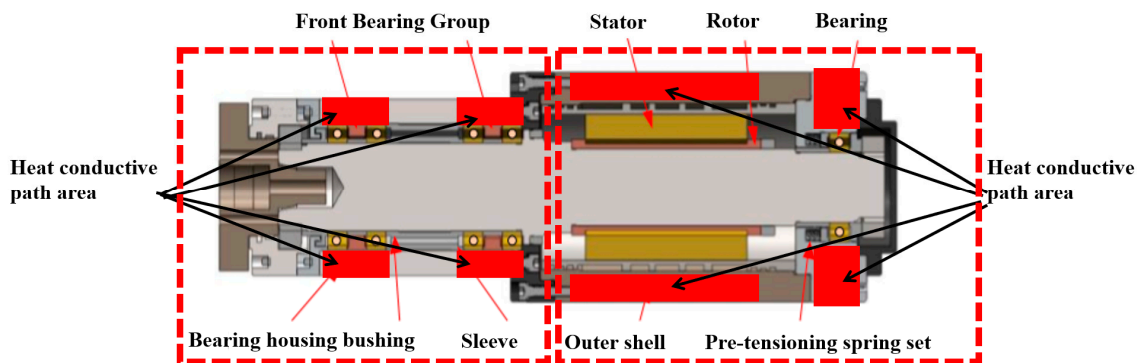
Figure 1. Design area for building heat conductive paths and its equivalent model.

The triangular grid was chosen for the division of the design area. Each cell was numbered according to the three nodes as shown in Figure 2.
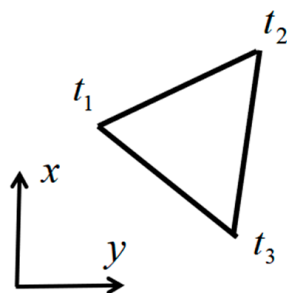
Figure 2. Planar three-node schematic.

For each triangular element of the design domain, the temperature interpolation function is:

$$T^e(x, y) = a_0 + a_1 x + a_2 y + a_3 xy = [N(x, y)]\{t_e\} \tag{1}$$

where $N(x, y)$ is the shape function of the cell, a_0, a_1, a_2, and a_3 are the coefficients to be determined, x and y are the node coordinates, T^e denotes the node temperature, and t_e denotes the node temperature array.

Usually, when performing finite element analysis, the more concentrated the units, the more accurate the results. However, too many units will put demands on the computer memory, and the longer the computation time, the lower the analysis efficiency. Therefore, in order to make the results reasonable, the elements should be densely divided in the place where the gradient of change of the analyzed target is obvious and the distribution is concentrated. The elements should be sparsely divided in the place where the gradient of change is small. Because the solution target is the heat dissipation weakness that is affected by temperature and the effect of the heat conductive path is to export the spindle heat radially, the unit close to the spindle was intensive and the one away from the spindle was disperse. Combined with the above analysis, the results of the mesh division of the annular channel region are shown in Figure 3.
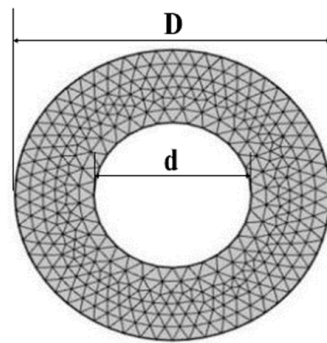

Figure 3. Grid division results.

The matrix B is given by:

$$B = \left\{ \begin{matrix} \frac{\partial T}{\partial x} \\ \frac{\partial T}{\partial y} \end{matrix} \right\} = \left\{ \begin{matrix} \frac{\partial}{\partial x}(a_0 + a_1 x + a_2 y + a_3 xy) \\ \frac{\partial}{\partial y}(a_0 + a_1 x + a_2 y + a_3 xy) \end{matrix} \right\} \tag{2}$$

After interpolation of the temperature field T, the shape function of the triangular unit cell is:

$$T = NT^e \tag{3}$$

$$N = \begin{bmatrix} N_1(x, y) & N_2(x, y) & N_3(x, y) & \dots & N_n(x, y) \end{bmatrix} \tag{4}$$

where n denotes the number of cells, N represents the interpolation function of each cell. The thermal conductivity of the material is expressed as follows.

$$k = \begin{pmatrix} k_x \\ k_y \end{pmatrix} = \begin{bmatrix} k_{xx} & 0 \\ 0 & k_{yy} \end{bmatrix} \tag{5}$$

According to the Galerkin method, Equation (3) was derived with the help of matrix notation. Then, the heat transfer matrix can be expressed as:

$$[K] = \iint_{\Omega} B^T Q B \mathrm{d}\Omega \tag{6}$$

where Ω and Q denote the design area and the thermal load matrix. Based on the law of conservation of energy and equations above, the centralized thermal conductivity model is established. The finite element equation can be expressed as:

$$\left[\iint_\Omega B^T Q B \mathrm{d}\Omega\right] T^e = \{f_Q\} \tag{7}$$

2.2. Mathematical Model

Heat was always conducted from a high-temperature object to a low-temperature object, and there was potential capacity dissipation in this process. The best heat dissipation was achieved if the potential capacity dissipation was minimized. Based on the heat transfer potential capacity dissipation principle [28], the expression for the heat dissipation weakness C in steady state can be obtained by combining the heat transfer equation derived from Equation (7) as:

$$C = \int_\Omega K_{ij} \frac{\partial T}{\partial x_i} \frac{\partial T}{\partial x_j} \mathrm{d}\Omega \tag{8}$$

Using the finite element method, the discretization is processed and the derivative is obtained as:

$$KT = P \tag{9}$$

$$\begin{aligned} K &= \sum_n \iint_e \tfrac{1}{2} T^{eT} B^T \lambda B T^e \mathrm{dxdy} \\ P &= \sum_n \iint_e T^{eT} N^T \rho q_v \mathrm{dxdy} \end{aligned} \tag{10}$$

where K denotes the heat transfer matrix of the overall structure and P denotes the amount of heat load on the overall structure.

In this paper, the heat dissipation weakness C is taken as the optimization objective to find the topological structure with the highest thermal conductivity for the structure. The discrete mathematical model was established as follows.

$$\begin{aligned} find \quad & x = \{x_1, x_2, \cdots x_n\} \in R^n \\ \min \quad & C = T^T KT = C = \sum_{e=1}^{n} T_e{}^T K_e T_e \\ s.t. \quad & \begin{aligned} & \sum_{e=1}^{n} x_e v_e \leq f \cdot V_0 \\ & KT = P \\ & 0 < x_{\min} \leq x_e \leq 1 \end{aligned} \end{aligned} \tag{11}$$

where C denotes the objective function, x is the cell design variable, T denotes the temperature vector within the design domain, v_e is the volume of the cell, V_0 is the total volume of the design domain, f denotes the material body fraction ratio. To save calculation time, the parameter $x_{\min}$ is artificially set as 0.001.

3. Topology Structural Design of Heat Conductive Path

Based on Section 2, the structure of heat conductive paths was designed. The flow chart of the topology optimization of the heat conductive path's structure is shown in Figure 4.

The basic parameters and working condition information were first determined in the process. Then, the heat dissipation weakness C was considered as the objective function of the iterative solution. The design variables were constantly updated and the location of the material distribution was determined. The specific iterative conditions were different because of different optimization methods. In the OC algorithm, the sensitivity was selected as the condition for filtering cells and in the IPTO algorithm, the density was selected as

the condition for filtering cells. When the result reached the set conditions, the loop was skipped. The topological structure calculation was completed.
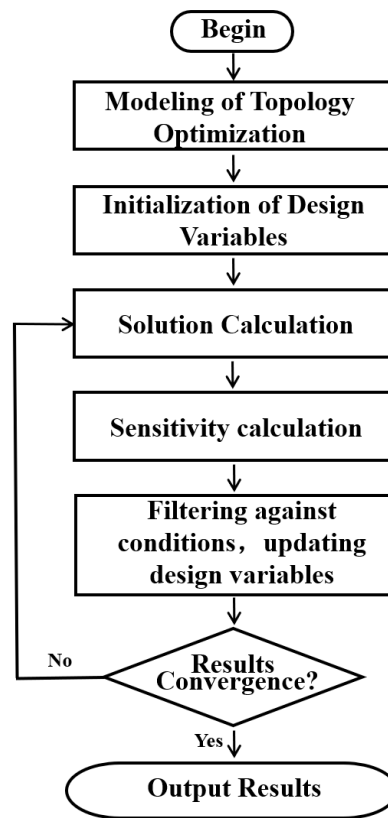
Figure 4. Flow chart of topology optimization of heat conductive path.

3.1. Topology Structural Design Based on OC Algorithm

According to Figure 4, the sensitivity analysis formula was derived from the interpolation function of the heat transfer unit. In solving topology optimization problems, the SIMP (Solid Isotropic Material with Penalization) model was used for interpolation calculation. The thermal conductivity coefficient of the unit can be interpolated as follows:

$$K_e = (x_e)^p K_0, e = 1, 2, 3, \ldots, n \tag{12}$$

where K_e and K_0 denote the material heat transfer coefficient of the unit and the penalized unit material heat transfer coefficient, x_e is the unit pseudo-density, and p is the penalty parameter, which is artificially taken as 3.

When iterating design variables, in order to improve computational efficiency and avoid checkerboard patterns, it was necessary to find design variables that change very little before and after the iteration. This process was called sensitivity analysis, and that was also to find the very small value of the objective function. When the SIMP method was used for interpolation, the sensitivity of the objective could be analyzed:

$$\frac{\partial C}{\partial x_e} = \sum_{e=1}^{n} -p(x_e)^{p-1} T_e^T k_{ex_e} T^e = 0 \tag{13}$$

In this section, the OC (Optimality Criteria) algorithm was used to perform an updated iterative calculation. The OC algorithm is a traditional optimization criterion method. This algorithm satisfies the optimization conditions for each iteration from the initial design point. According to the iterative formula, an improved design variable is obtained.

In order to find the optimal distribution path of the material in the design domain, it was necessary to find the minimum value of the heat dissipation weakness. It was transformed into an extreme value problem with constraints, which can be obtained by combining the discrete mathematical model (11) in Section 2 and the Lagrange function:

$$L = C(x_i) + \lambda_1 \left(\sum_{i=1}^{n} V_i x_i - V_0 \right) + \lambda^+ \int_{\Omega} (x_i - 1) dx + \lambda^- \int_{\Omega} (x_{\min} - x) dx \qquad (14)$$

where x_i denotes the value of the design variable calculated in the *i*-th iteration, and λ_1, λ^+, and λ^- denote the introduced Lagrange multipliers.

According to the Kuhn–Tucker condition, the derivation of the above equation yielded the stationary value condition on λ_1, λ^+, and λ^-.

$$\begin{cases} \frac{\partial L}{\partial x_i} = \frac{\partial C}{\partial x_i} + \lambda_1 \frac{\partial V}{\partial x_i} + \lambda^+ + \lambda^- \begin{cases} \leq 0, x_i \geq 1 \\ = 0, x_{\min} \leq x_i \leq 1 \\ \geq 0, x_i \leq x_{\min} \end{cases} \\ \begin{cases} \sum_{i=1}^{n} V_i x_i - V_0 \leq 0 \\ \lambda \sum_{i=1}^{n} V_i x_i - V_0 = 0 \end{cases}, \lambda_1 \geq 0 \\ \begin{cases} x_{\min} - x_i \leq 0 \\ \lambda^- (x_{\min} - x_i) = 0 \end{cases}, \lambda^- \geq 0 \\ \begin{cases} x_i - 1 \leq 0 \\ \lambda^+ (x_i - 1) = 0 \end{cases}, \lambda^+ \geq 0 \end{cases} \qquad (15)$$

Too many discrete cells led to too many design variables, thus making it difficult to solve Equation (15). Therefore, the following iterative updating strategy was generally used for the computation:

$$x_i^{nem} = \begin{cases} \max(x_{\min}, x_i - m), if (x_i B_i^{\eta})^q \leq \max(x_{\min}, x_i - m) \\ (x_i B_i^{\eta})^q, if \max(x_{\min}, x_i - m) \leq (x_i B_i^{\eta})^q \leq \min(1, x_i + m) \\ \min(1, x_i + m), if \min(1, x_i + m) \leq (x_i B_i^{\eta})^q \end{cases} \qquad (16)$$

where $x_{\min}$ is the lower limit of the parameter, which is set to prevent the matrix singularity, m ($0 < m < 1$) is the step length limit and η ($0 < \eta < 1$) is the damping factor, and $(x_i B_i^{\eta})$ denotes the sensitivity filter function. The expression B_i is shown below:

$$B_i = \frac{\frac{\partial C(x_i)}{x_i}}{\lambda_1 \frac{\partial V(x_i)}{x_i}} \qquad (17)$$

Based on the OC algorithm, the topology optimization design of the heat conductive path for the model was proposed. The initial value of the ambient reference temperature was set as T_0 = 298 K. Thermal conductivity of heat conductive path was λ = 401 W/(m²·K), the volume proportion *V* of heat conductive paths was set as 10–40%, the penalty parameter *p* = 3, and the lower limit of material density was set to 0.001 (kg/m³). Then, the thermal conductivity paths with different volume proportions were obtained and are shown in Figure 5.

It can be seen from Figure 5 that as the volume proportion increased from 10 to 40%, the number of main branches of the heat conductive paths was 16. When the volume proportion was low, the main branches were divided into branches with multiple levels while as the volume proportion increased, the veins of the main branches became fewer. The diameter of the main branches increased from 14 mm to 18 mm.
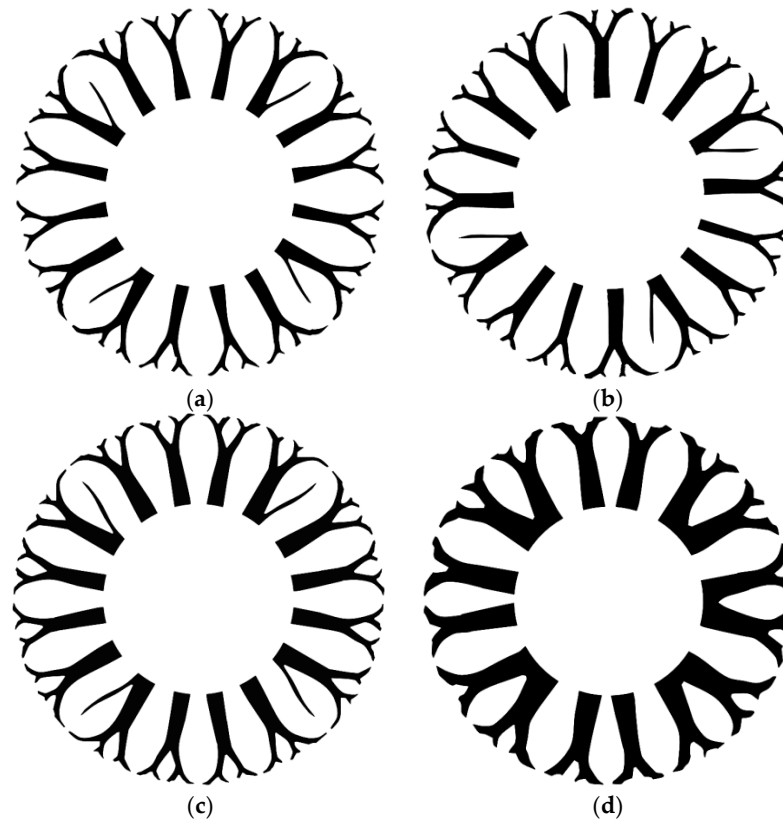
Figure 5. Topological structure of heat conductive paths based on the OC algorithm. (**a**) V = 10%; (**b**) V = 20%; (**c**) V = 30%; (**d**) V = 40%.

3.2. Topology Structural Design Based on IPTO Algorithm

IPTO (Improved Proportional Topology Optimization) is a corrected proportional optimization algorithm [29]. For the uncertain variables in the design process, first filter those which obey the normal distribution of the variables and then correct them. Finally, the corrected variables are considered as the design parameters so that the sensitivity analysis of the design variables can be ignored. The filtering of the design variables can be carried out through the idea of probability to make the design variables nearer to 0/1 faster in the iteration process.

The IPTO algorithm has the advantages of not needing to obtain sensitivity information, fast convergence, and strong ability to obtain the exact solution. Taking the heat dissipation weakness C as the optimization objective, the following discrete mathematical model can be established based on the IPTO algorithm.

$$
\begin{aligned}
find \quad & x = \{x_1, x_2, \cdots x_n\} \in R^n \\
\min \quad & C = T^T K T = C = \sum_{e=1}^{n} T_e^T K_e T_e \\
s.t. \quad & \sum_{e=1}^{n} x_e v_e \leq f \cdot V_0 \\
& KT = P \\
& x_{\min} \leq x \leq x_{\max}
\end{aligned}
\tag{18}
$$

where $x_{\min}$ and $x_{\max}$ are the upper and lower boundary values of the discrete cell x_e, respectively.

The SIMP penalty model was used as the material interpolation model in the IPTO algorithm, which can be expressed as follows:

$$
E_e = E_{\min} + x_e^p (E_0 - E_{\min})
\tag{19}
$$

where E_0 and E_{min} are the thermal conductivity of the solid and void materials, respectively, and E_{min} is taken as 0.001 to avoid a singular matrix.

The filtering of the SIMP interpolation model was performed using a weighted average of:

$$\begin{cases} \widetilde{x}_e = \frac{1}{\sum\limits_{j \in N_e} H_e} \sum\limits_{j \in N_e} H_{e,j} x_e \\ H_{e,j} = \max\{0, R_{min} - d_{e,j}\} \end{cases} \tag{20}$$

where $\widetilde{x}_e$ is the filtered density variable of discrete cell e, and N_e is the cell set, which is formed by the sweep of the discrete cell j with the discrete cell e as the center and R_{min} as the filtering radius. x_j is the density variable of discrete cell, $H_{e,j}$ and $d_{e,j}$ are the weight coefficient and distance between discrete cells, respectively.

After the update of the density variable in the inner loop of IPTO algorithm, the density variable x_e^{pre} obtained in the last iteration was introduced into the main loop for a density variable update. The update of main loop density variable was implemented using the following equation:

$$x_e^{nem} = \alpha x_e^{pre} + (1 - \alpha) x_e^{pre} \tag{21}$$

where x_e^{pre} and x_e^{nem} are the discrete cell density variable obtained from the previous iteration and the current iteration of the main cycle density variable update, and α is the scale factor.

Based on the IPTO algorithm, the topology structural design was obtained. The relevant parameters, such as temperature and thermal conductivity of material, were set as the same as Section 3.1. As shown in Figure 6, the thermal conductive paths of the model with different volume proportions were obtained. Similarly, it can be seen from the figure below that as the volume proportion increased from 10% to 40%, the number of main branches increased from 7 to 16. The diameter of the largest main branch increased from 6 to 20 mm and the number of branching structures decreased.
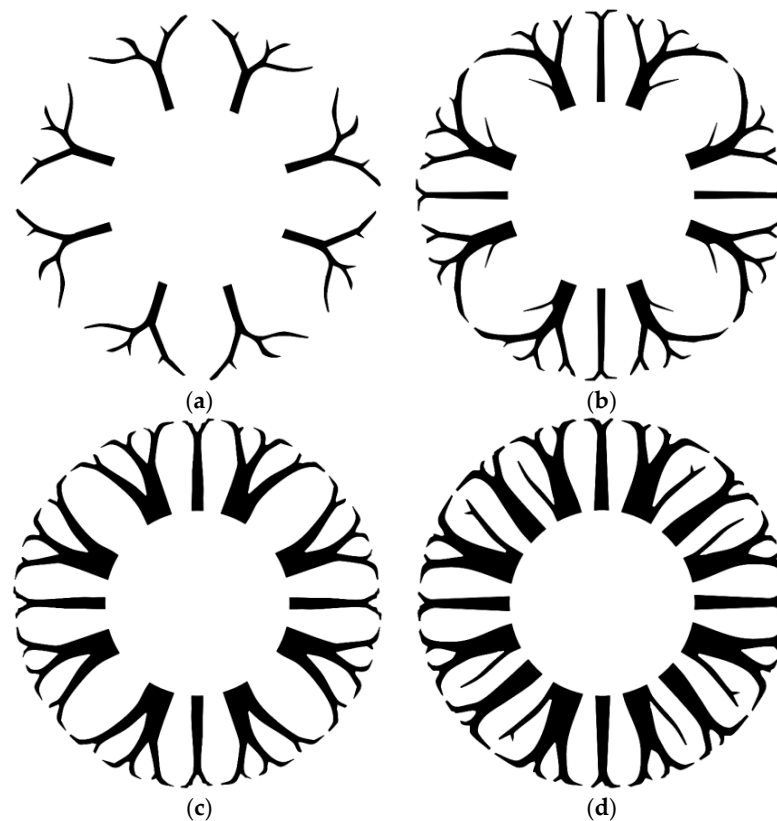

Figure 6. Topological structure of heat conductive paths based on IPTO algorithm. (**a**) V = 10%; (**b**) V = 20%; (**c**) V = 30%; (**d**) V = 40%.

4. Thermal Characteristics and Stress Strength Analysis of Models with Heat Conductive Paths

4.1. Numerical Model

In order to analyze the influence of the heat conductive path on the circumferential heat distribution of the spindle, a toroidal 3D model was built (see Figure 7). The outer radius d_1 was 160 mm, the inner radius d_2 was 80 mm, and the thickness δ was 20 mm. In Figure 7a, it is a normal toroidal model without heat conductive paths, and in Figure 7b, it is a toroidal model with topology structure of heat conductive paths based on OC algorithm (volume proportion of copper V = 10%).
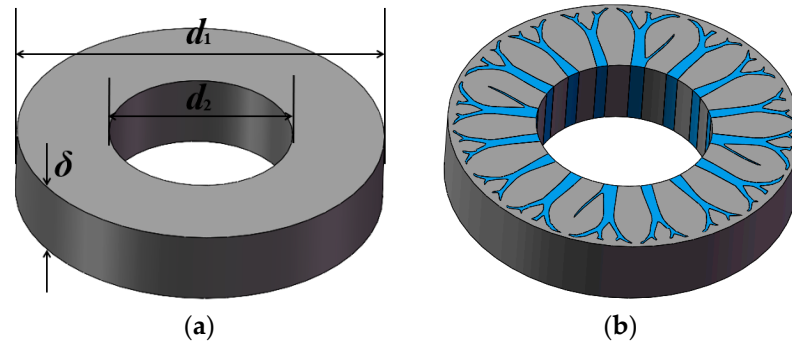
Figure 7. Toroidal 3D model. (**a**) General toroidal model; (**b**) Toroidal model with topology.

The material of the heat conductive path was copper, and the rest of the model was set to structural steel. The material properties are shown in Table 2.

Table 2. Thermal boundary conditions of heat conductive path model.

Materials	Density(g/cm^3)	Thermal Conductivity (W·m^{-1}K^{-1})	Thermal Expansion Coefficient (m/$^\circ$C)
Steel	7.85	50.2	1.2×10^{-5}
Copper	8.969	401	1.67×10^{-5}

In this paper, tetrahedral cell type is selected for meshing (see Figure 8). The mesh of the heat conductive path in the model was refined. The average quality of the mesh was 0.85.
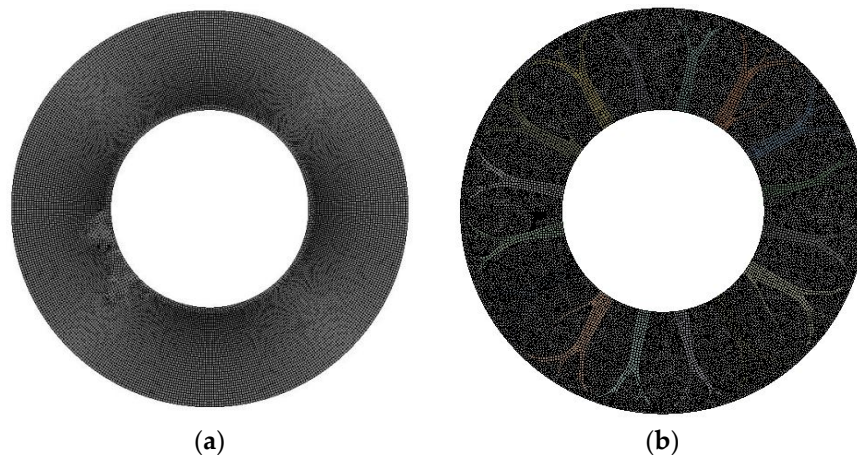
Figure 8. Meshing result. (**a**) General toroidal model; (**b**) Toroidal model with topology.

Using the method proposed by Palmgren, the heat generation of the outer ring of 7010C angular contact bearing was calculated. When the spindle speed was 12,000 r/min, the heat generation of the bearing outer ring heating was 149 W and heat flow density

$q_{bearing}$ = 39,734 W/m^2. For calculation convenience, $q_{bearing}$ was taken as 40,000 W/m^2 and loaded on surface of the inner ring. The outer ring of the model was set as a constant temperature boundary, T_{out} = 25 °C.

4.2. Thermal Characteristics Simulation of Heat Conductive Path

Based on the ANSYS-Workbench software platform, thermal characteristics of the models were analyzed. The thermal steady state simulation results of model without heat conductive paths (pure structural steel), and with heat conductive paths (topology optimized structure based on OC algorithm and IPTO algorithm) are shown in Figures 9–11. The heat conductive path was filled with high thermal conductivity material (copper) and its volume proportion was increased from 10% to 40%.
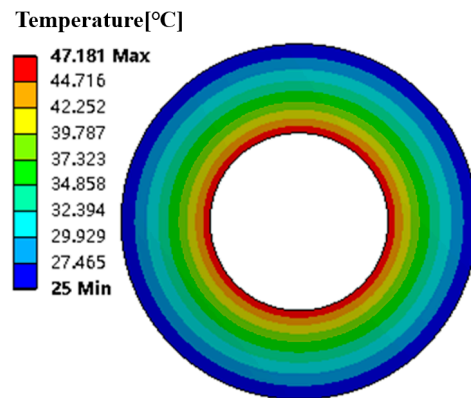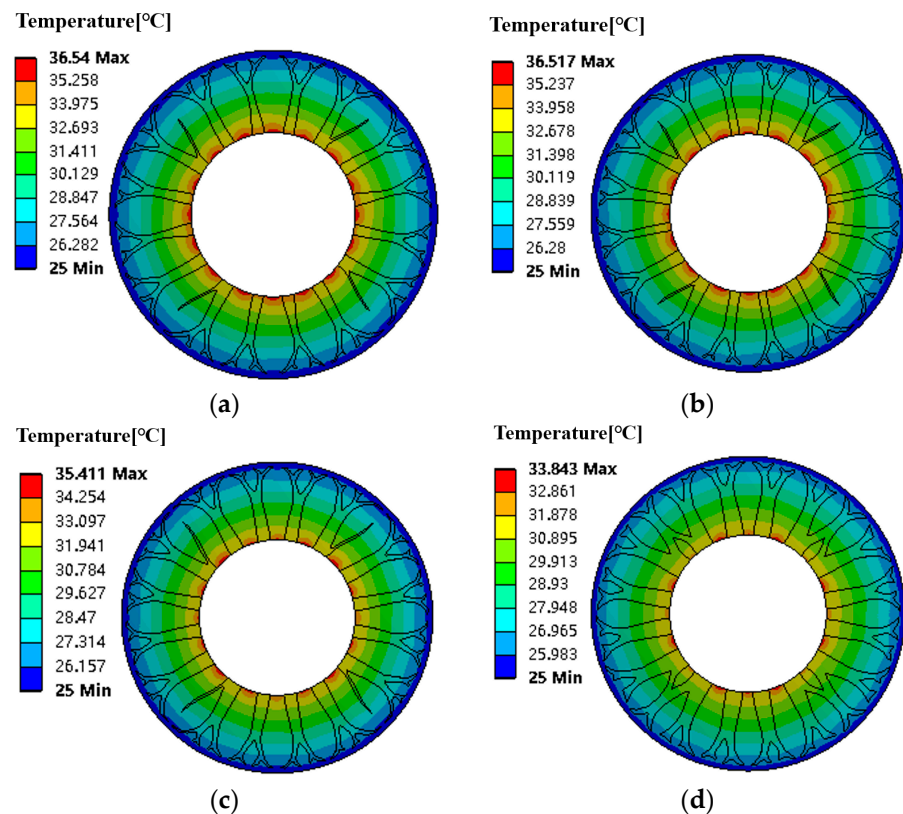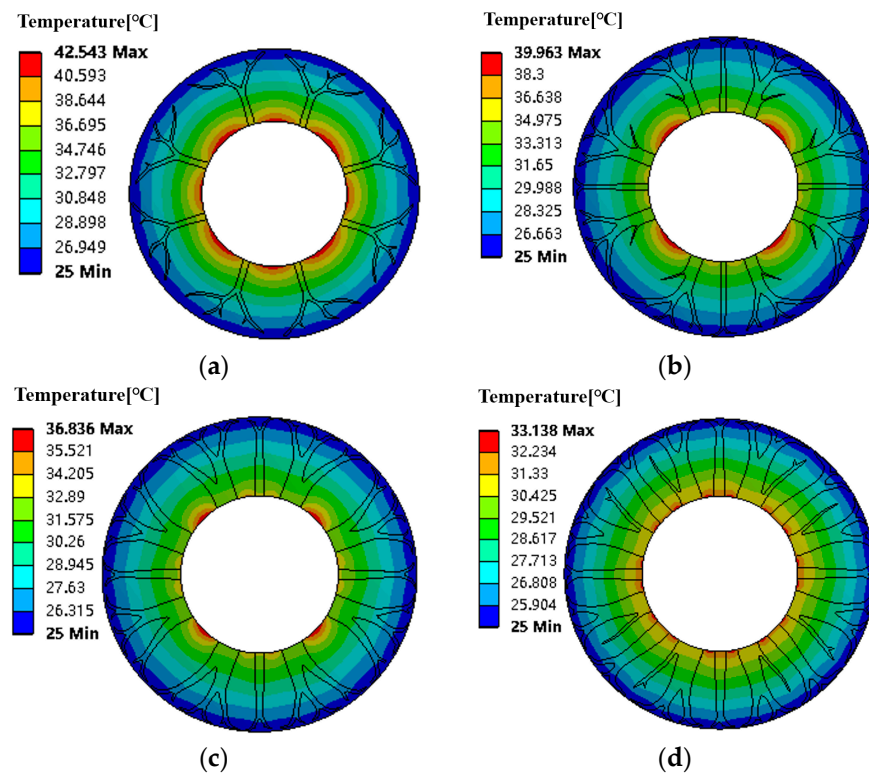

Figure 9. Toroidal 3D model.

Figure 10. Simulation result of the model with heat conductive path (based on the OC algorithm). (**a**) Copper volume proportion V = 10%; (**b**) Copper volume proportion V = 20%; (**c**) Copper volume proportion V = 30%; (**d**) Copper volume proportion V = 40%.

Figure 11. Simulation result of the model with heat conductive path (based on the IPTO algorithm). (**a**) Copper volume proportion V = 10%; (**b**) Copper volume proportion V = 20%; (**c**) Copper volume proportion V = 30%; (**d**) Copper volume proportion V = 40%.

As shown in Figure 9, when there was no heat conductive path, the temperature of the toroidal model decreased gradually from inside to outside. The high temperature area was uniformly distributed around the inner ring. The temperature of the inner ring was the highest 46.8 °C, and the temperature of the outer ring was the lowest 25 °C. For the toroidal model with topological heat conductive paths, the temperature distribution was similar with to model without heat conductive path, but the high temperature areas were obviously concentrated in the inner ring. From Figures 9–11, it can be seen that the maximum temperature with the heat conductive path was significantly lower. The temperature rises under the thermal steady state decreased obviously when the topological structure of the heat conductive path was adopted.

However, the difference of thermal conductivity of the two topology structures based on OC and IPTO algorithm cannot be seen clearly. Therefore, the steady-state temperatures of two different topology structures were compared specifically.

As shown in Figure 12, with the increase of the copper volume proportion, the maximum temperature of the model decreased. As the volume proportion of the copper increased from 10% to 40%, the maximum temperature with heat conductive path based on the OC algorithm decreased from 36.5 °C to 33.8 °C and the maximum temperature with heat conductive path based on the IPTO algorithm decreased from 42.5 °C to 33.1 °C.

When the proportion of copper in the total volume was less than 40%, the thermal conductivity of the topological structure based on IPTO algorithm was higher. When the volume proportion of copper was 10%, the steady-state temperature difference between the heat conductive paths under the two algorithms was the largest, which was 6 °C. When the volume proportion of copper was 40%, the thermal conductivity of models and the steady-state temperature based on the OC and IPTO algorithms was close. This meant that when the volume proportion was high, thermal conductivity materials reached a certain value, the difference in thermal conductivity caused by different topological structures was no longer obvious.
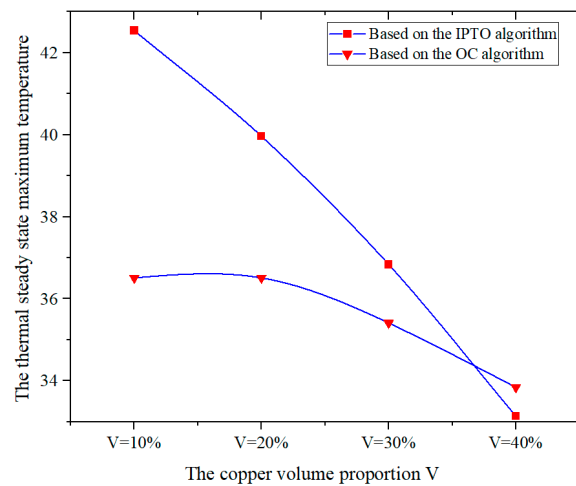
Figure 12. Comparison of the thermal steady state maximum temperature rise of the heat conductive path with topology.

4.3. Stress Strength Analysis of Heat Conductive Path

In order to verify the strength performance of the structure, the coupled static-thermodynamic analyses of heat conductive path based on the OC and IPTO algorithms were carried out respectively. The path was mainly subjected to radial load as well as its own gravity, and the axial load was calculated to be 700 N.

It can be seen from Figures 13 and 14 that the maximum stress of the heat conductive path based on the OC algorithm was 3.0445 MPa when the copper volume proportion was 10%. The maximum stress of the heat conductive path based on the IPTO algorithm was 2.2116 MPa when the copper volume proportion was 20%. The bearing radial force induced by the stress was mainly along the horizontal direction of the distribution, manifested in the stress of the left end being bigger than the right end and the stress of the inner circle being bigger than the outer ring. The stress was mainly distributed in the area where copper and structural steel came into contact with each other.
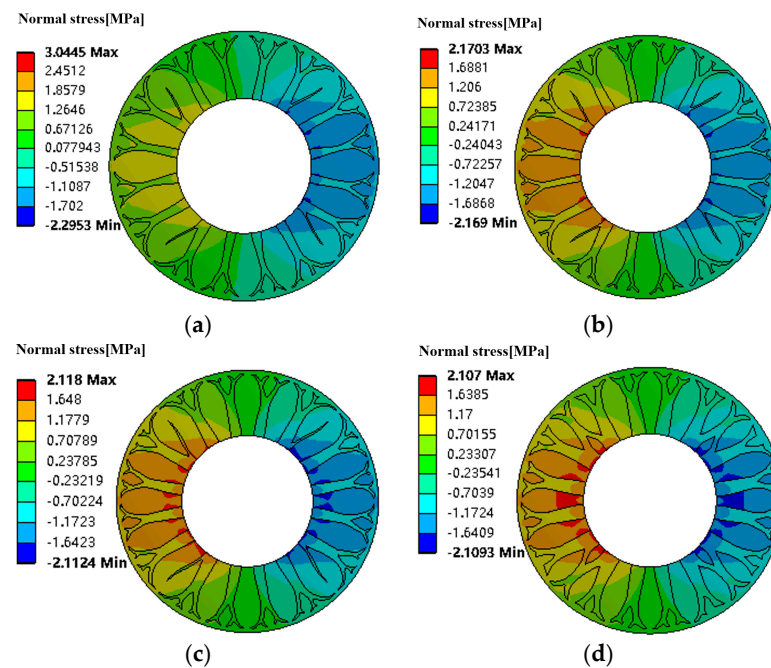

Figure 13. Stress analysis results of the model with heat conductive path (based on the OC algorithm). (**a**) Copper volume proportion V = 10%; (**b**) Copper volume proportion V = 20%; (**c**) Copper volume proportion V = 30%; (**d**) Copper volume proportion V = 40%.
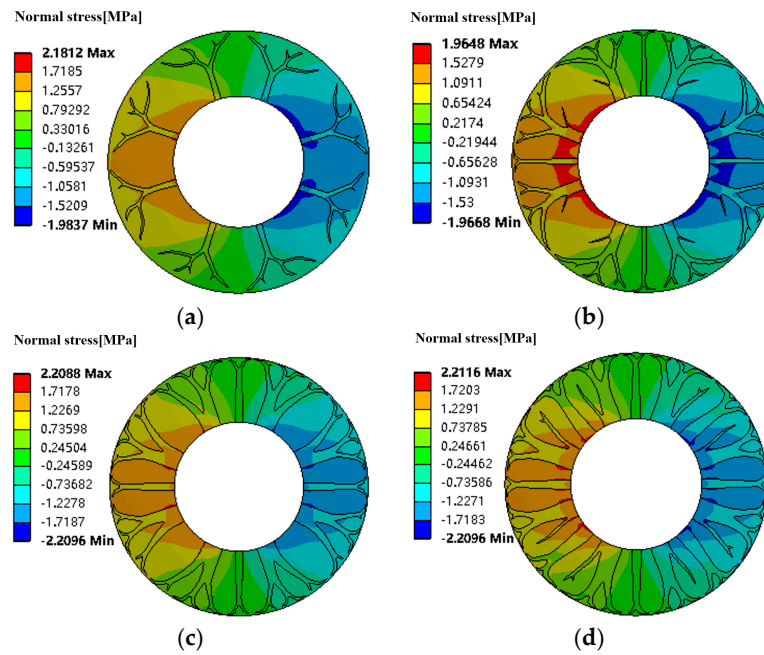
Figure 14. Stress analysis results of the model with heat conductive path (based on the IPTO algorithm). (**a**) Copper volume proportion V = 10%; (**b**) Copper volume proportion V = 20%; (**c**) Copper volume proportion V = 30%; (**d**) Copper volume proportion V = 40%.

However, the difference of stress strength of the two topology structures based on the OC and the IPTO algorithm cannot be seen clearly. Therefore, the normal stress of two different topology structures was compared specifically.

As shown in Figure 15, the stress change of the heat conductive path based on the IPTO algorithm was basically out of a U-shape and the size of the fluctuation range was small and relatively stable. The stress change of the heat conductive path based on the IPTO algorithm decreased fast when copper volume proportion increased from 10% to 20%. The stress decreased from 3.0 MPa to 2.1 MPa, and then showed a stable trend. From the overall point of view, the stress was below 3 MPa, and the value of the stress was small, which had no effect on the heat dissipation effect.
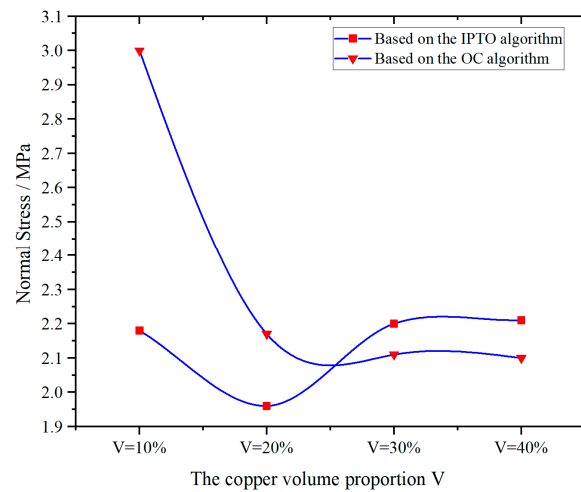
Figure 15. Comparison of the stress change of the heat conductive path with topology.

5. Conclusions

In order to enhance the heat dissipation of the spindle system, the heat conductive path was constructed. With heat conductive path filling with high thermal conductivity materials, the heat generated by the bearing inside the spindle could be quickly exported. By using the OC and IPTO algorithms, topology structures with different volume proportions of the high thermal conductivity material were obtained. As the volume proportion increased, the number of main branches of the topology structure increased and the diameter of the largest main branch increased but the number of branching structures decreased. Based on the thermal characteristics simulation results, it was found that the heat conductive path with topology can effectively reduce the temperature rise. Compared with the normal model, the highest temperature of the model with heat conductive path (the volume proportion of the copper was 40%) decreased from more than 47 °C to less than 34 °C. As the volume proportion of the copper increased from 10% to 40%, the maximum temperature with heat conductive path based on the OC algorithm decreased from 36.5 °C to 33.8 °C and the maximum temperature with heat conductive path based on the IPTO algorithm decreased from 42.5 °C to 33.1 °C. However, when the volume proportion of copper reached 40%, the thermal conductivity of models and the steady-state temperature based on these two algorithms were close. It can be seen that in the range of copper volume proportion from 10% to 40%, the heat dissipation effect of the heat conductive path based on the OC algorithm was better than that based on the IPTO algorithm. At the same time, the maximum stress on the topological structure was less than 3 MPa, which did not affect the heat dissipation effect and met the actual working conditions.

Author Contributions: Validation, Z.H.; Formal analysis, L.L.; Investigation, W.H.; Writing—original draft, Y.L.; Writing—review & editing, Z.L.; Supervision, W.W.; Project administration, W.Z. All authors have read and agreed to the published version of the manuscript.

Data Availability Statement: There is no new data were created, or the data is unavailable due to privacy or ethical restrictions.

References

1. Li, Y.; Yu, M.L.; Bai, Y.M.; Hou, Z.Y.; Wu, W.W. A Review of Thermal Error Modeling Methods for Machine Tools. *Appl. Sci.* **2021**, *11*, 5216. [CrossRef]
2. Ma, Y.M.; Cui, H.Y.; Li, C.C.; Wu, C.Z.; Zhao, Z.Y. Thermal Error Measurement and Analysis of Vertical Machining Center. *MATEC Web Conf.* **2019**, *256*, 03005. [CrossRef]
3. Wang, H.T.; Li, T.M.; Wang, L.P.; Li, F.C. Review thermal error modeling of machine tools. *J. Mech. Eng.* **2015**, *51*, 119–128. [CrossRef]
4. Li, Z.L.; Wang, Q.H.; Zhu, B.; Wang, B.D.; Zhu, W.M. Thermal error modeling of high-speed electric spindle based on Aquila Optimizer optimized least squares support vector machine. *Case Stud. Therm. Eng.* **2022**, *39*, 102432. [CrossRef]
5. Mayr, J.; Jedrzejewski, J.; Uhlmann, E.; Donmez, M.-A.; Knapp, W.; Härtig, F.; Wendt, K.; Moriwaki, T.; Shore, P.; Schmitt, R.; et al. Thermal issues in machine tools. *CIRP Ann.* **2012**, *61*, 771–791. [CrossRef]
6. Liu, Y.; Wang, X.F.; Zhu, X.G.; Zhai, Y. Thermal error prediction of motorized spindle for five-axis machining center based on analytical modeling and BP neural network. *J. Mech. Sci. Technol.* **2021**, *35*, 281–292. [CrossRef]
7. Ji, P.; Ming, Y.; Li, C.; Liao, Q.H.; Wang, L.; Yin, G.F. Study on the spindle axial thermal error of a five-axis machining center considering the thermal bending effect. *Precis. Eng.* **2022**, *75*, 210–226.
8. Deng, X.L.; Lin, H.; Wang, J.C.; Xie, C.X.; Fu, J.Z. Review on thermal design of machine tool spindles. *Opt. Precis. Eng.* **2018**, *26*, 1415–1429. [CrossRef]
9. Li, M.Y.; Ma, C.; Zeng, S.; Hu, J.L.; Wang, S.L. Cooling water jacket design of motorized spindle system using multi-objective topology optimization. *Appl. Therm. Eng.* **2023**, *224*, 120112. [CrossRef]

10. Donmez, M.-A.; Hahn, M.-H.; Soons, J.-A. A novel cooling system to reduce thermally-induced errors of machine tools. *CIRP Ann.* **2007**, *56*, 521–524. [CrossRef]
11. Huo, D.H.; Kai, C.; Wardle, F. A holistic integrated dynamic design and modelling approach applied to the development of ultraprecision micro-milling machines. *Int. J. Mach. Tools Manuf.* **2010**, *50*, 335–343. [CrossRef]
12. Zhou, S.B.; Chen, L.G.; Sun, F.R. Volume-point Conduction Optimization of Variable Cross-section Conducting Path Based on Constructal Theory. *J. Mech. Eng.* **2008**, *44*, 46–50. [CrossRef]
13. Chen, W.J.; Liu, S.T.; Zhang, Y.C. Optimization design of conductive pathways for cooling a heat generating body with high conductive inserts. *Chin. J. Theor. Appl. Mech.* **2016**, *48*, 406–412.
14. Cheng, X.G.; Li, Z.X.; Guo, Z.Y. Construction of Efficient Heat Conductive Path Based on Biomimetic Optimization. *Sci. China Ser. E* **2003**, *33*, 251–256.
15. Peng, Y. Study of Bionic Vapor Chamber Based on the Plant Leaf Structure. Ph.D. Thesis, South China University of Technology, Guangzhou, China, 2015.
16. Wang, R.; Yin, Y.; Xie, Z.H.; Chen, L.G.; Wu, F.; Li, W.L. Constructal design of elliptical cylinder heat generation components under natural convection. *Energy Conserv.* **2019**, *8*, 27–31.
17. Li, W.L.; Xie, Z.H.; Xi, K.; Guan, X.N.; Ge, Y.L. Constructal Optimization of Double-layered Microchannel Heat Sink with Porus Side Fins. *Semicond. Optoelectron.* **2021**, *42*, 364–370.
18. Sigmund, O. Tailoring materials with prescribed elastic properties. *Mech. Mater.* **1995**, *20*, 351–368. [CrossRef]
19. Diaz, A.-R.; Sigmund, O. A topology optimization method for design of negative permeability metamaterials. *Struct. Multidiscip. Optim.* **2010**, *41*, 163–177. [CrossRef]
20. Guest, J.-K.; Prévost, J.-H. Design of maximum permeability material structures. *Comput. Methods Appl. Mech. Eng.* **2007**, *196*, 1006–1017. [CrossRef]
21. Musaddiq, A.-A.; Masatoshi, S. Investigation of concurrent multiscale topology optimization for designing lightweight macrostructure with high thermal conductivity. *Int. J. Therm. Sci.* **2022**, *179*, 107653.
22. Wu, S.H.; Zhang, Y.C.; Liu, S.T. Topology optimization for minimizing the maximum temperature of transient heat conduction structure. *Struct. Multidiscip. Optim.* **2019**, *60*, 69–82. [CrossRef]
23. Burger, F.-H.; Dirker, J.; Meyer, J.-P. Three-dimensional conductive heat transfer topology optimisation in a cubic domain for the volume-to-surface problem. *Int. J. Heat Mass Transf.* **2013**, *67*, 214–224. [CrossRef]
24. Long, K.; Jia, J. Periodic Topology Optimization Design for Thermal Conductive Structure Using ICM Method. *Eng. Mech.* **2015**, *32*, 227–235.
25. Long, K.; Wang, W.W.; Jia, J. Topology Optimization for Microstructures of Materials with Macrostructure Property Constraint. *Acta Mater. Compos. Sin.* **2016**, *33*, 1574–1583.
26. Zhao, X.; Liu, Y.C.; Fang, Z.; Hu, P.; Zhou, M.D. Topology Optimization of the Cross-section Layout of Channel-cooling Tools. *Chin. J. Comput. Mech.* **2019**, *36*, 597–602.
27. Fan, Y.S. Heat Dissipation Structure Optimization Topology Design Based on SIMP Power Device IGBT. Master's Thesis, Guilin University of Electronic Technology, Guilin, China, 2020.
28. Cheng, X.G.; Li, Z.X.; Guo, Z.Y. Heat Conduction Optimization Based on Least Dissipation Principle of Heat Transport Potential Capacity. *J. Eng. Thermophys.* **2003**, *24*, 94–96.
29. Wang, H.; Cheng, W.M.; Zhai, S.C.; Peng, Q.H. Reliability-based topology optimization of continuum structure with the IPTO algorithm. *Mod. Manuf. Eng.* **2021**, *12*, 105–111.